

THE YUAN-TSEH LEE ARRAY FOR MICROWAVE BACKGROUND ANISOTROPY

PAUL T.P. HO^{1,2}, PABLO ALTAMIRANO¹, CHIA-HAO CHANG¹, SHU-HAO CHANG¹, SU-WEI CHANG¹, CHUNG-CHENG CHEN¹, KE-JUNG CHEN¹, MING-TANG CHEN¹, CHIH-CHIANG HAN¹, WEST M. HO¹, YAU-DE HUANG¹, YUH-JING HWANG¹, FABIOLA IBÁÑEZ-ROMANO¹, HOMIN JIANG¹, PATRICK M. KOCH¹, DEREK Y. KUBO¹, CHAO-TE LI¹, JEREMY LIM¹, KAI-YANG LIN¹, GUO-CHIN LIU^{1,3}, KWOK-YUNG LO^{1,4}, CHENG-JIUN MA^{1,5}, ROBERT N. MARTIN^{1,6}, PIERRE MARTIN-COCHER¹, SANDOR M. MOLNAR¹, KIN-WANG NG¹, HIROAKI NISHIOKA¹, KEVIN E. O'CONNELL¹, PETER OSHIRO¹, FERDINAND PATT¹, PHILIPPE RAFFIN¹, KEIICHI UMETSU^{1,7}, TASHUN WEI¹, JIUN-HUEI PROTY WU^{8,7}, TZI-DAR CHIU⁸, TZIHONG CHIU^{8,7}, TAH-HSIUNG CHU⁸, CHIH-WEI LOCUTUS HUANG^{8,7}, W.Y. PAUCHY HWANG^{8,7}, YU-WEI LIAO^{8,7}, CHUN-HSIEN LIEN⁸, FU-CHENG WANG^{8,7}, HUEI WANG⁸, RAY-MING WEI⁶, CHIA-HSIANG YANG⁸, MICHAEL KESTEVEN⁹, JEFF KINGSLEY¹⁰, MALCOLM M. SINCLAIR⁹, WARWICK WILSON⁹, MARK BIRKINSHAW¹¹, HAIDA LIANG^{11,12}, KATY LANCASTER¹¹, CHAN-GYUNG PARK¹³, UE-LI PEN¹⁴, & JEFFREY B. PETERSON¹⁵

Draft version September 12, 2021

ABSTRACT

The Yuan-Tseh Lee Array for Microwave Background Anisotropy (AMiBA) is the first interferometer dedicated to studying the cosmic microwave background (CMB) radiation at 3mm wavelength. The choice of 3mm was made to minimize the contributions from foreground synchrotron radiation and Galactic dust emission. The initial configuration of seven 0.6m telescopes mounted on a 6-m hexapod platform was dedicated in October 2006 on Mauna Loa, Hawaii. Scientific operations began with the detection of a number of clusters of galaxies via the thermal Sunyaev-Zel'dovich effect. We compare our data with Subaru weak lensing data in order to study the structure of dark matter. We also compare our data with X-ray data in order to derive the Hubble constant.

Subject headings: cosmology: cosmic microwave background — instrumentation: interferometers — telescopes

1. INTRODUCTION

The Yuan-Tseh Lee Array for Microwave Background Anisotropy (AMiBA)¹⁶ is a platform-mounted 7-element interferometer operating at 3-mm wavelength to study the structure of the cosmic microwave background (CMB) radiation. It is being constructed as part of the Cosmology and Particle Astrophysics (CosPA) Project, funded by the Taiwan Ministry of Education Initiative on Academic Excellence. This Excellence Initiative was aimed at stimulating interdisciplinary research and large scale integration of independent research programs. CosPA is designed to jump start a program of research in cosmology, with both theory and experimental projects, while incorporating research in high energy physics, development of infrastructure for optical astronomy in Taiwan, as well as accessing observing time on a 4-m class opti-

cal telescope.

AMiBA is a collaboration between principally the Academia Sinica Institute of Astronomy and Astrophysics (ASIAA), the National Taiwan University (NTU) Physics and Electrical Engineering Departments, and the Australia Telescope National Facility (ATNF). The project was started in 2000. A two-element prototype was deployed in 2002 to Mauna Loa (elevation 3396m) in Hawaii for testing of design concepts. Site development was completed in 2004. The AMiBA mount was delivered and installed in 2004, while the platform was delivered and integrated in 2005. With the integration of the first seven elements of the array and successful first light, the AMiBA was dedicated in October 2006, and named after then Academia Sinica President Yuan Tseh Lee for his important contributions in promoting the growth of astronomy in Taiwan. Figure 1 shows the AMiBA at the dedication ceremony.

The aim of AMiBA is to study spatial structure in the CMB radiation (Ho et al. 2008; Wu et al. 2008a), which carries imprints of various physical processes in early epochs of the Universe. Since its initial detection by Penzias & Wilson (1965), the CMB has been recognized as the definitive signature of the Big Bang which began the expansion of the Universe. Subsequent studies have established the properties of this relic radiation after its decoupling from the matter in the early universe around $z \simeq 1100$: a mean temperature of 2.725K (present) with minute fractional anisotropies at the level of 10^{-5} (COBE, Mather et al. 1990; Smoot et al. 1992), and polarization at the level of a few to 10% of temperature fluctuations (DASI, Kovac et al. 2002; WMAP, Kogut et al. 2003; Page et al. 2007; Nolte et al. 2008; CBI, Readhead et al. 2006; QUaD, Pryke et al. 2008). In particular, the CMB structures seen on various angular scales by COBE and then WMAP (Bennett et al. 2003; Spergel et al. 2007; Komatsu et al. 2008) demonstrated that the angular power spectrum of CMB anisotropies is a powerful probe of our cos-

¹ Academia Sinica Institute of Astronomy and Astrophysics, P.O. Box 23-141, Taipei 10617, Taiwan

² Harvard-Smithsonian Center for Astrophysics, 60 Garden Street, Cambridge, MA 02138, USA

³ Tamkang University, Tamsui, Taipei County, Taiwan 251

⁴ National Radio Astronomy Observatory, Edgemont Road, Charlottesville, VA 22903, USA

⁵ IfA, University of Hawaii at Manoa, 2680 Woodlawn Dr., Honolulu, HI, 96822

⁶ Composite Mirror Applications, Tucson, AZ 85710, USA

⁷ Leung center for Cosmology and Particle Astrophysics, National Taiwan University, Taipei 10617, Taiwan

⁸ National Taiwan University, Taipei 10617, Taiwan

⁹ Australia Telescope National Facility, Epping, NSW Australia 1710

¹⁰ Steward Observatory, University of Arizona, Tucson, AZ 85721, USA

¹¹ University of Bristol, Tyndall Avenue, Bristol BS8 1TL, UK

¹² Nottingham Trent University, Burton Street, Nottingham NG1 4BU, UK

¹³ Sejong University, Seoul, 143-747, Korea

¹⁴ Canadian Institute for Theoretical Astrophysics, Toronto, ON M5S 3H8, Canada

¹⁵ Carnegie-Mellon University, Pittsburgh, PA 15213 USA

Electronic address: pho@asiaa.sinica.edu.tw, ho@cfa.harvard.edu

¹⁶ <http://amiba.asiaa.sinica.edu.tw/>

mological model of the Universe. AMiBA is built to sample the angular range from $2'$ to $20'$, corresponding to spherical harmonic multipoles $l = 800\text{--}8000$, at a wavelength of 3 mm, with full polarization. These capabilities complement existing, on-going, and planned experiments. The angular scales sampled by AMiBA address the higher-order acoustic peaks of the CMB structures to further constrain cosmological models. AMiBA also aims to search for, and study, distant high-redshift clusters of galaxies whose hot intracluster gas will distort the CMB spectrum via the thermal Sunyaev Zel'dovich effect (hereafter SZE, Sunyaev & Zel'dovich 1970, 1972; Rephaeli 1995; Birkinshaw 1999; Carlstrom, Holder, & Reese 2002). The optical and X-ray surface brightnesses of clusters of galaxies decrease rapidly with increasing redshift due to cosmological redshift dimming, while the detectable SZE is close to being independent of redshift because it is a spectral distortion of the CMB radiation which itself increases in intensity with increasing redshift as $T_{\text{CMB}}(z) \propto (1+z)$ in a standard cosmological model. Thus SZE measurements are potentially more sensitive than X-ray observations for finding clusters of galaxies beyond a redshift $z \sim 1$, and will be an important probe for the matter distribution in the high-redshift universe.

In this paper, we describe the design and construction of AMiBA, the first observational results, and the scientific potential of this instrument. Throughout this paper, we adopt a concordance Λ CDM cosmology with $\Omega_m = 0.3$, $\Omega_\Lambda = 0.7$, and $h \equiv H_0/(100 \text{ km s}^{-1} \text{ Mpc}^{-1}) = 0.7$.

2. DESCRIPTION OF THE INSTRUMENT

The basic characteristics of AMiBA are summarized in Table 1.

2.1. Design, Construction, and Performance of AMiBA

Interferometry at 3 mm

With the funding of the CosPA/AMiBA projects in 2000, a workshop was held to define the scientific objectives and the design of AMiBA (Lo et al. 2001; Liang 2002). *The first design criterion was to operate at 3-mm wavelength.* This was to take advantage of the sweet spot at 3 mm where the fractional SZE decrement with respect to the primary CMB is close to its maximum (see Figure 1 of Zhang et al. 2002) and the SZE signal is minimally-contaminated by the Galactic synchrotron emission, dust foregrounds, and the population of cluster and background radio sources. Operations at 3 mm also complement the wavelength coverage of other existing and planned CMB instruments: interferometers such as CBI at 30 GHz (Padin et al. 2002), AMI at 15 GHz (Scaife et al. 2008), SZA (Mroczkowski et al. 2008)¹⁷ at 30 and 90 GHz, and VSA at 30 GHz (Watson et al. 2002); bolometer arrays such as ACT,¹⁸ APEX-SZ (Halverson et al. 2008),¹⁹ and SPT.²⁰

The second design criterion was to choose interferometry. This was a somewhat difficult choice as many new CMB projects were then planning to use bolometer arrays, which held the promise of a greater inherent sensitivity because of the broad wavelength coverage and a greater speed because of the multiple elements of the detector arrays. The choice of interferometry was based on the desire to utilize cross correlations to suppress systematic effects, since the ability for

bolometers to integrate down to theoretical noise was unknown at that point. Furthermore, ASIAA had the experience of working in millimeter wavelength interferometry from being a partner on the Submillimeter Array (SMA) project (Ho et al. 2004). AMiBA was seen as an extension and application of the technical capabilities within ASIAA. Interferometry is also a natural way to sample simultaneously the spatial structures on various scales and to construct a map by Fourier inversion. Imaging the entire primary beam of the individual elements of an interferometer is equivalent to a multi-element detector array.

Platform Mounted Interferometer and Hexapod Drive

The third design criterion concerns the angular sizes to be pursued. AMiBA was specifically designed to sample structures in the CMB on small angular scales at multipoles $l = 800\text{--}8000$, complementing in angular scales earlier large-sky CMB experiments (e.g., COBE, MAXIMA, BOOMERANG) and the DASI experiment on degree/sub-degree angular scales ($l = 140\text{--}900$; Leitch et al. 2002a, 2002b). In the left panel of Figure 2, we show the initial compact configuration of seven 0.6 m antennas (*small solid circles*) on the 6 m platform (*solid outer circle*), along with the distribution of holes (*crosses*) for mounting receiver packages. At each of the frequency channels centered at about 90 and 98 GHz, this compact configuration provides 21 simultaneous baselines with three baseline lengths of $d = 0.61, 1.05, \text{ and } 1.21$ m, corresponding to angular multipoles $l = 2\pi\sqrt{u^2 + v^2} (\equiv 2\pi d/\lambda)$ of $l \approx 1194, 2073, 2394$ at $\nu_c = 94$ GHz. Also shown in the right panel of Figure 2 is the sensitivity of the 7-element compact array as a function of $l = 2\pi d/\lambda$ at two frequency channels, represented by window functions (see eq. [14] of White et al. 1999) for the three different baseline-lengths. For the initial configuration of AMiBA at 3 mm (see Figures 2 and 3), we are sensitive to the multipole range of $800 \lesssim l \lesssim 3000$, which roughly overlaps with the CBI experiment at 1 cm^{-21} (Padin et al. 2002; Mason et al. 2003; Pearson et al. 2003) but is complementary in observing frequency. Hence AMiBA aimed at angular scales from 2 to 20 arcmin, in order to extend the coverage of angular sizescales by one more order of magnitude. The choice of 3-mm wavelength meant the required baselines were 0.6 m to 6 m. A maximum baseline of 6 m immediately suggested that this interferometer is small enough to be mounted on a platform, as pioneered by CBI and DASI.

The fourth design criterion was therefore to choose a carbon fiber platform for weight and stiffness considerations. The platform was made with multiple holes for mounting the receiver packages, to accommodate multiple baseline configurations. The layout of the receiver ports has a hexagonal pattern in order to allow close packing, and also to utilize the triangular patterns used by small interferometers such as the SMA, CBI, and DASI, in order to achieve the most uniform uv -coverage. An ASIAA team led by Robert N. Martin and Philippe Raffin designed the platform, which was manufactured by Composite Mirrors Applications. A single rigid platform has the advantages of stable differential pointing, a stable baseline solution without differential delay tracking, no mutual shadowing by individual reflectors, and a single drive system. However, a platform also means the interferometer does not have different projected baselines because of earth

¹⁷ <http://astro.uchicago.edu/sza/>

¹⁸ <http://www.hep.upenn.edu/act/act.html>

¹⁹ <http://bolo.berkeley.edu/apexsz>

²⁰ <http://pole.uchicago.edu>

²¹ The achieved angular resolution of the 7-element compact AMiBA is similar to CBI, but the primary beam FWHM of CBI is about twice larger than that of AMiBA.

rotation.

The fifth design criterion was the choice of a hexapod mount, which provides six degrees of freedom (which are tightly constrained) in driving the telescope and rotating the platform. By rotating the reflectors with respect to the celestial source, additional uv -spacings are sampled. The rotation of the platform, described by the so-called polarization angle of the platform, also allows us to set different orientations of the receivers relative to the ground, which is useful for discriminating between various environmental effects and checking for ground pick-up. These capabilities were introduced both by CBI and DASi, and we have incorporated them. The hexapod mount was designed and built by Vertex Antennentechnik, Duisburg, Germany. To protect the telescope from the elements, we use a retractable shelter with seven steel trusses covered with a PVC fabric, which is manufactured by American Spaceframe Fabricator Inc.

Reflectors

The individual parabolic reflectors are built in carbon fiber in order to minimize their weight. The choice of 0.6m (0.576m, to be precise) for the reflector diameter was driven by the desire to cover angular sizescales from 2–20 arcmin in order to extend and overlap with existing CMB data. The choice of 1.2m for the diameter of the second-generation reflectors was to increase the collecting area and to improve the spatial dynamic range and angular resolution for SZE observations while utilizing the entire platform. The reflectors were designed by ASIAA, and manufactured by CoTech, Taichung, Taiwan. The design includes baffles to shield against crosstalk between individual elements, and Gortex covers to shield against direct solar irradiation. The height of the baffles is approximately 30% of the diameter of the reflectors so that the secondary mirrors are well shielded. The supports for the secondary are attached to the baffles which are attached to the edges of the primary. Replicating an accurate carbon fiber surface against a steel mold was not simple, and some hand polishing was required. Depositing the actual reflecting surface and a protective coating was also not simple especially for the 1.2m size. Nevertheless, a collaborative effort between ASIAA and CoTech was successful in delivering the reflectors with surface accuracy better than 50 microns. This is 2% of the operating wavelength of 3mm, and would allow efficient operation up to 1mm. Laboratory measurements and outdoor beam pattern measurements showed that the performances of the reflectors met the specifications (for details see Koch et al. 2006).

Receiver System

The sixth design criterion was to choose heterodyne receiver systems, which operate between 86 and 102 GHz. This choice of frequency covers an excellent region of atmospheric transparency. The design, construction, and integration of the receiver systems were performed by ASIAA staff led by Ming-Tang Chen. Dual polarization capabilities are provided by waveguide orthomode transducers, which follow the circular corrugated feedhorns and the circular-to-linear polarizers. Each polarization is then fed into a JPL monolithic-microwave-integrated-circuit (MMIC) InP HEMT low noise amplifier (LNA) cooled to 15 K with standard CTI22 refrigerators. These LNAs performed well with measured noise temperatures of 35–50 K across a 20 GHz bandwidth (Weinreb et al. 1999). We used subharmonically pumped mixers

(SHM) using the same MMIC technology. The LO/IF systems are designed and built by Tah-Hsiung Chu and his group at the NTU EE-department. The phase-locked LO signal at 21 GHz is doubled to 42 GHz and then phase switched with Walsh functions before being combined with the sky signal at the SHM. Variable attenuators and amplifiers, before and after mixing, control the IF levels before correlation. Slope equalizers, phase stabilized cables, and adjustable delays are used to further adjust the IF signals. We measure the effective receiver temperatures across the 2–18 GHz IF window to be 55–75 K. Figure 3 shows the AMiBA fully loaded with all the receivers and correlator modules. More details on the receiver system are given by Chen et al. (2008).

Correlator System

The seventh design criterion was to choose a wide band correlator with analog technology. This is a joint development effort between ASIAA and ATNF, with Chao-Te Li, Derek Kubo, and Warwick Wilson leading the effort (Li et al. 2004). A digital correlator would have required sampling at too high a rate to be practical. The AMiBA correlator uses balanced diode mixers to multiply the signals from each pair of antennas. After application of the 4 different lags, the cross-correlated signal is then digitized and read out with integrated circuits designed by Tzi-Dar Chiueh of the NTU EE department. The readout ICs demodulate the phase-switched signals and accumulate the counts for specified times. The choice of a small number of lags is to reduce bandwidth smearing effects while maintaining the maximum bandwidth response through the cascade of electronics. The bandwidth smearing effect is described by the product of the fractional bandwidth and the displacement of the source from the field center. A 10% bandwidth will keep the distortion below 20% (5%) at the FWHM of the primary beam of the 0.6m (1.2m) reflectors. Because of the small number of lags to cover a large bandwidth, the conversion to complex visibility is strongly affected by gain variations over the pass-band, differential delays between lags, and non-linear phase response for each lag. The lag-to-visibility transformation is calibrated with a noise source. This is discussed further by Lin et al. (2008).

Drive System and Pointing

The hexapod drive system is more complex than the conventional azimuth-elevation drive systems used in radio astronomy. The difficulty lies in the necessity of driving all six hexapod jacks without over-extension or collisions. Vertex Antennentechnik provided the control software. The performance of the drive system was checked via pointing and tracking tests (Koch et al. 2008a). Pointing of the AMiBA utilized an optical telescope mounted on the platform. We identified a misalignment of the anchor cone and the mount, tilt of the optical telescope with respect to the mount, flexure in the platform as a function of the platform polarization angle, and local platform deformation. We also measured the repeatability of pointing on both short and long timescales, and we performed photogrammetry to measure the stability of the platform. Pointing was found to be repeatable at the 4'' level on a timescale of several hours. The absolute rms pointing error appears to be about 0.8' for the platform set at zero polarization angle, and up to 3' if the platform is allowed to rotate to different polarization angles. However, with the implementation of an interpolation table, absolute rms pointing can be reduced to 0.4' over all sky. This is less than 10%

of the primary beams of the 0.6m reflectors, and is within specifications for the operation of the 7-element compact array (Koch et al. 2008a). However, when the 1.2m reflectors are deployed, pointing needs to be improved by a factor of 2.

Deformation of the Platform

The segmented approach instead of a monolithic design for our carbon fiber platform resulted in unforeseen difficulties. The bolted joints between the six outer segments were not stiff enough. In spite of efforts to strengthen the joints with additional plates and brackets, the platform still deforms under operational loads to a level beyond our specifications. A saddle-shaped deformation pattern is present with an amplitude dependent on the hexapod azimuth, elevation and polarization position. Fortunately, the deformation appears repeatable when measured with photogrammetry which means that it can be modeled. Maximum deformation at the edge of the platform under simulated full loading is 0.38mm. The maximum deformation in the inner 3m of the platform is more modest at 0.120mm, and within specifications for the operation of the 7-element compact array. The deformation is due principally to the platform not being stiff enough, and also because the stresses from the drive system are transmitted to the platform in spite of a steel interface ring (Koch et al. 2008a). The immediate ramification is that the individual primary beams of the interferometer elements will be mis-pointed relative to each other. This is equivalent to the primary mirror of a single dish telescope being deformed under gravity or atmospheric distortion. The equivalent adaptive optics approach for an interferometer involves adjusting the gains and phases of the individual elements either through a look-up table or via self calibration if the signals are strong enough. The advantage of an interferometer is that we can adjust the signals during the postprocessing phase before adding or multiplying the signals from different baselines. For our current configuration, such correction schemes for the platform deformation do not need to be implemented.

System Performance

Calibration of the AMiBA system was led by Kai-Yang Lin and Chao-Te Li. The receiver temperatures were measured by the standard hot/cold load method to be 55 to 75 K. The contribution from the sky and ground pickup to the total system temperatures is about 25 K. Since the correlator only has 4 lags, only 2 frequency channels can be extracted. The response of the correlator is therefore not easy to measure, and we use planets to calibrate the correlator response periodically. We find the complex gain to be stable to 5% in gain and 0.1 rad in phase on time scales of a few hours.

Using the detected fluxes for Saturn and Jupiter, the overall system efficiency was estimated to be 0.3–0.4 for each of the baselines of the interferometer. This efficiency accounts for all losses due to illumination, blockage, spillover, alignment of the reflectors with respect to the radio axis of the platform, deformation of the platform, and pointing, as well as the narrower correlator response (Lin et al. 2008). The losses in front of the receiver account for the significant contributions from the sky and ground pickup to the system temperatures. In two-patch differencing observations a sensitivity of about 63 mJy is achieved in 1 hour of on-source integration under good sky conditions (Chen et al. 2008; Lin et al. 2008).

Gaussianity of the Noise

Since the SZE signals and the CMB anisotropy are quite faint, the behavior of the noise is very important. This analysis has been led by Hiroaki Nishioka. We conducted tests of blank sky data as well as data where the inputs are terminated by absorbers. Statistical analysis of different samples of such data showed no significant differences. Time variable signals from the correlator due to electronics and ground pickups can be seen in the various datasets. However, a power spectrum analysis demonstrated white noise behavior for frequencies between 10^{-4} and 1 Hz. Hence two-patch differencing of the sky signal at 600 sec intervals is adequate to remove the slowly varying contaminations.

By cross correlating the outputs from the different lags of the correlator, we find only a weak correlation at less than 10%. By dividing the datasets into smaller samples, we verify that the sample variance is consistent with Gaussian random noise which would integrate down over time. We also applied the Kolmogorov-Smirnov (K-S) test to our cluster data, and we find that 90% of the data are consistent with Gaussian behavior at the 5% significance level. The data which fail the test at 5% level are often found to be associated with hardware problems, and we use this criterion to discard questionable samples. More details on the Gaussianity tests are given in Nishioka et al. (2008).

Contamination on the Observed SZE Signals

Since the SZE signals are faint, they can be confused with the CMB anisotropies and foreground emission structures. The analysis of possible contaminations has been led by Guochin Liu. Examining the WMAP data, we can see that CMB structures on the scale of a degree are suppressed by our two-patch observing technique, while contamination from Galactic emission is typically fainter than the CMB emission by an order of magnitude. From WMAP data, we also estimate possible contamination from primary CMB anisotropies, by analyzing 500 simulated CMB fields, for the sizescales which we sample. We find contamination at the level of 13 to 90 mJy for the sampled multipoles of $l = 1200$ to 2400 (at 94 GHz).

We also estimated potential contamination from foreground point sources. The best way to correct for this issue is to have high angular resolution interferometer data at the observed frequencies. Lacking such data, we extrapolate the contributions from known point sources in low frequency radio surveys. Since spectral indices are not known accurately to 3 mm, a statistical approach is used to estimate the contamination in each cluster from known point sources. In all clusters, a net positive contribution of the point sources was found in our main-trail/lead differencing AMiBA observations, indicating that there are more radio sources towards clusters than in the background (as expected; see Coble et al. 2007). The corrections for contamination are described more fully in Liu et al. (2008).

2.2. First Science Results from the AMiBA

First Light

First light with the 7-element AMiBA was achieved in September 2006. The array of 0.6m reflectors was in the close-packed configuration on the platform (Figures 2 and 3). The image of Jupiter shown in Figure 4 is the first end-to-end test of the system based on drift-scan data, including the pipeline for data analysis. The image was constructed from drift scans at four equally-divided platform polarization angles to provide better uv -coverage. Only the transit data of

about 0.23 s exposure time from each drift scan were used, yielding an overall noise level in the dirty map of about 3 Jy, much lower than the Jupiter flux density of 844 Jy. Successful images were obtained for Saturn, Venus, and the Crab Nebula, all with fluxes on the order of 200 Jy. In particular, the measured angular size of the Crab Nebula is consistent with existing optical and radio images. In December 2006, using Saturn as the calibrator, Uranus was imaged with a flux density of 11 ± 4 Jy (at 2σ confidence level; in 16 1 s exposures), consistent with the expected level of 7.3 Jy.

Imaging Clusters of Galaxies

At the achieved sensitivity, the close-packed 7-element configuration of AMiBA is suitable for imaging galaxy clusters via the SZE. During 2007, we imaged 6 clusters, chosen to be relatively nearby (a median redshift of $z \sim 0.2$), already detected in SZE, and resolvable with AMiBA. Target selection and data analysis are described in Wu et al. (2008b). To detect the much fainter SZE signals from clusters of galaxies, we need to integrate longer. At this level of sensitivity, emission from local terrestrial sources such as buildings and the ground will enter through the system either through the sidelobes of the antenna response or via scattering into the primary beam. The interferometer has the advantage over a bolometer array in that the cross correlation will suppress extended low level emission which enters the system through the sidelobe response of the reflectors. However, structures on angular scales corresponding to the interferometer baselines will still persist. The design of the baffles around the edges of the reflectors helps further suppression, but we did not exercise the option of installing ground shields. Instead we employ a two- or three-patch observing technique where the target source is preceded and/or followed by tracking over the same range of azimuth and elevation just traversed by the source. This allows us to subtract and cancel the terrestrial ground and sky emission. This is the AMiBA equivalent of the position-switching technique used in single-dish radio astronomy, where we track specifically the same part of the atmosphere. As shown in Figure 5, and in Wu et al. (2008b), this procedure is quite successful and we have mapped the SZE decrement towards a number of clusters. These detections serve to demonstrate the scientific potentials of AMiBA.

Distribution of Mass and Hot Baryons in Cluster Environment

AMiBA will be sensitive to structures as large as $20'$ with resolution as high as $2'$ so that SZE structures can be resolved. Even at the current angular resolution of $6'$ FWHM, an extended, elliptical shape can be seen for some of the clusters. These shapes can be compared to the results from weak gravitational lensing or X-ray imaging. The SZE and X-ray images are sensitive to the distribution of the hot intracluster gas, while the weak lensing images probe the distribution of all the gravitational mass including the dominant “invisible” dark matter. Furthermore, the X-ray emission is sensitive to the square of the electron density while the SZE measures the thermal electron pressure projected along the line-of-sight, linearly tracing the electron column density. Hence, the complementary X-ray, the SZE, and the weak lensing data, probe progressively further out in the mass distribution.

For four of the massive clusters in our sample (A1689, A2142, A2261, A2390), for which high-quality Subaru weak lensing data are available, we have compared the SZE results with the Subaru weak lensing measurements (Umetsu

et al. 2008). In the case of Abell cluster A2390, the elliptical shape seen in SZE is consistent with the shape of the dark matter distribution as deduced from weak lensing data.

For this comparison, A2142 is of particular interest since this is our brightest, most-nearby (resolvable) SZE cluster at $z = 0.091$, known as a merging cluster with two X-ray *cold fronts*, which are sharp edges in X-ray dense cores (Markevitch et al. 2000). In Figure 6 we compare for A2142 our AMiBA SZE map with the projected mass distribution (*white contours*) as deduced from our weak lensing analysis. Here the mass map is smoothed to a resolution of $2'$ FWHM. Our AMiBA SZE map shows an elliptical structure extending in the northwest (NW) - southeast (SW) direction, similar to X-ray and weak lensing distribution shapes (Figure 6; see also Figure 10 of Okabe & Umetsu 2008). The almost $20'$ angular extent of the cluster SZE justifies the use of observing with antennas as small as 0.6 m, so that the observations are sensitive to large scale structures. Further, relative positions (between pixels) are important in such maps of extended structures, where the interferometer has the inherent advantage of relying on the phase to determine relative positions, while single dish studies might be affected more strongly by pointing of the telescopes.

In the cluster A2142, a mass subclump located $\sim 10'$ ($\sim 710 \text{ kpc} h^{-1}$ at the cluster redshift) to the NW of the cluster center has been detected from the Subaru weak lensing analysis of Okabe & Umetsu (2008) and Umetsu et al. (2008). This NW mass subclump, lying $\sim 5'$ ahead of the NW-edge of the X-ray dense core, has no X-ray counterpart in Chandra and XMM-Newton observations, but is associated with a slight excess of cluster sequence galaxies (see Figure 10 of Okabe & Umetsu 2008). Our AMiBA map exhibits slight excess SZE signals in the NW region (Figure 6) at $2 - 2.5\sigma$ significance levels. We note this slight excess SZE appears extended over a couple of synthesized beams, although the per-beam significance level is marginal. Good consistency found between the SZE and weak lensing maps is encouraging, and may suggest that the NW excess SZE is a pressure increase in the ICM associated with the moving NW substructure. Clearly further improvements in both sensitivity and resolution of the SZE mapping (see §2.3) are needed to better constrain the merger geometry and physical properties of the merging substructure. This however demonstrates the potential of SZE observations as a powerful tool for measuring the distribution of ICM in cluster outskirts where the X-ray emission measure ($\propto n_e^2$) is less sensitive. This also demonstrates the potential and reliability of AMiBA, and the power of multiwavelength cluster analysis for probing the distribution of mass and baryons in clusters.

Finally, for our small sample with a mean virial mass of $\langle M_{\text{vir}} \rangle = (1.2 \pm 0.1) \times 10^{15} M_{\odot} h^{-1}$, the hot gas mass fraction is about $(13 \pm 3)\%$ (Umetsu et al. 2008). As compared to the cosmic baryon fraction $f_b = \Omega_b / \Omega_m$ of $\simeq 17\%$, as deduced from the WMAP 5-year data (Dunkley et al. 2008), possibly $(22 \pm 16)\%$ of the baryons are missing from the hot cluster environment (Umetsu et al. 2008). This missing cluster baryon fraction is partially made up by observed stellar and cold gas fractions of \sim several % in our X-ray temperature range ($T_X > 8 \text{ keV}$).

Estimating the Hubble Constant

By comparing the SZE and X-ray imaging results, we can deduce a value for the Hubble constant H_0 . Since the SZE is induced by inverse-Compton scattering of the CMB photons

by hot electrons in the cluster environment, it is sensitive to the total column of electrons. The X-ray emission is due to the Bremsstrahlung process between protons and electrons, and is therefore sensitive to the square of the electron density. By combining these two relations, the angular diameter distance can be deduced. However this derivation, and the subsequent measurement of H_0 depends on the assumed geometry of the emission region. We have derived a value of H_0 from our sample of SZE results combined with X-ray data. The uncertainty is high because of the small size of our sample, and the bias from the assumed geometry. However, the deduced value is consistent with other SZE constraints, and is an indicator of integrity of the AMiBA data so far. Better limits will come with a much larger sample to be obtained in the future.

2.3. Expansion to 13-elements

While the initial 7-element 0.6 m reflectors have been commissioned, we are proceeding with the expansion of the AMiBA to its 13-element configuration. In this configuration, we will upgrade from 0.6 m to 1.2 m antennas. This will increase the collecting area by a factor of ~ 7.4 , and the speed of the interferometer by a factor of almost 60 in single pointed observations. We will place the 13 elements over the platform to generate the longest possible baselines, which will result in angular resolutions up to $2'$. The correlator is also being expanded in order to handle the larger number of cross correlations.

In this second phase of AMiBA operations, the first science target will be to measure the angular power spectrum of CMB temperature anisotropies to the higher multipole numbers in order to examine the shape at and beyond the third acoustic peak ($l \sim 800$; Nolta et al. 2008), where data taken with the 7-element close-pack 0.6 m configuration will be combined with upcoming 13-element 1.2 m data. Accurate measurements of the angular power spectrum of CMB temperature anisotropies (Park et al. 2003) through $l \sim 4000$ up to $l \sim 8000$ will allow us to see secondary effects such as the SZE (Lin et al. 2004) and possible cosmic string structures (Wu 2004). The second science target will be to resolve cluster SZE structures on the sky in order to compare with dark matter structures as deduced from weak gravitational lensing studies (Umetsu & Futamase 2000; Broadhurst et al. 2005, 2008; Umetsu & Broadhurst 2008; Okabe & Umetsu 2008). The third science target will be to survey for the distribution of galaxy clusters

via the SZE (Zhang et al. 2002; Umetsu et al. 2004). To obtain redshifts of cluster candidates, optical follow up observations will be conducted with ground-based telescopes.

At the time of the publication of this paper, the expansion is already in progress. We anticipate first operations during 2009.

3. CONCLUSION

In this introductory paper, we have presented the design and construction of the Yuan-Tseh Lee AMiBA project. The telescope is now in scientific operation, and the first science results are the detection and imaging of six galaxy clusters via the Sunyaev Zel'dovich effect. Our companion papers elaborate on various aspects of our results. Chen et al. (2008) describe the technical design of the instruments in detail. Wu et al. (2008b) describe the observations and data analysis for the first year of AMiBA SZE data. Lin et al. (2008) examine the system performance, and discuss the astrophysical properties of planetary calibrators. Koch et al. (2008a) describe the performance of the hexapod mount and the carbon fiber platform. Nishioka et al. (2008) examine the integrity of the AMiBA data and its statistical properties. Liu et al. (2008) address the issues of foreground and primary-CMB contamination in AMiBA SZE observations. Umetsu et al. (2008) discuss the combination of AMiBA SZE and Subaru weak lensing data in order to probe the structure of dark matter and to derive the cluster gas mass fractions. Koch et al. (2008b) derive the value of the Hubble constant H_0 from AMiBA and X-ray data on the clusters. Huang et al. (2008) derive cluster scaling relations between the SZE and X-ray observables. Finally, Molnar et al. (2008) discuss the potential of AMiBA data in its 13-element configuration to constrain the intra-cluster gas distributions.

We thank the Ministry of Education, the National Science Council, and the Academia Sinica for their support of this project. We thank the Smithsonian Astrophysical Observatory for hosting the AMiBA project staff at the SMA Hilo Base Facility. We thank the NOAA for locating the AMiBA project on their site on Mauna Loa. We thank the Hawaiian people for allowing astronomers to work on their mountains in order to study the Universe.

REFERENCES

- Bennett, C. et al. 2003, ApJS, 148, 1
 Birkinshaw, M. 1999, Phys Rep, 310, 97
 Broadhurst, T., Takada, M., Umetsu, K., Kong, X., Arimoto, N., Chiba, M., & Futamase, T. 2005, ApJ, 619, L143
 Broadhurst, T., Umetsu, K., Medezinski, E., Oguri, M., & Rephaeli, Y. 2008, ApJ, 685, L9
 Carlstrom, J.D., Holder, G.P., and Reese, E.D. 2002, ARAA., 40, 643
 Chen, M.-T. et al. 2008, ApJ, submitted
 Coble, K., Bonamente, M., Carlstrom, J. E., Dawson, K., Hasler, N., Holzappel, W., Joy, M., La Roque, S., Marrone, D. P., & Reese, E. D. 2007, AJ, 134, 897
 Dunkley et al. 2008, submitted to ApJS, preprint (arXiv:0803.0586)
 Halverson, N.W. et al. 2008, ApJ, submitted (arXiv: 0807.4208)
 Ho, P.T.P., Moran, J.M., & Lo, K.Y. 2004, ApJ, 616, L1
 Ho, P.T.P. et al. 2008, Modern Physics Letter A, 23, 1243
 Huang, C.-W. L. et al. 2008, in preparation (ApJ companion paper)
 Koch, P. et al. 2008a, ApJS, submitted
 Koch, P. et al. 2008b, ApJ, in preparation
 Koch, P. et al. 2006 in *Proceedings of The European Conference on Antennas and Propagation: EuCAP 2006* (ESA SP-626), eds.: H. Lacoste & L. Ouweland. Published on CDROM., p.668.1
 Kogut, A. et al. 2003, ApJS, 148, 161
 Komatsu, E. et al. 2008, ApJS submitted (arXiv:astro-ph/08030547)
 Kovac, J.M., et al. 2002, Nature, 420, 772
 Leitch, E.M. et al. 2002a, ApJ, 568, L28
 Leitch, E.M. et al. 2002b, Nature, 420, 763
 Li, C.-T. et al. 2004 in *Millimeter and Submillimeter Detectors for Astronomy II*, ed. J. Zmuidzinas, W. Holland, and S. Withington, SPIE, Bellingham, WA
 Liang, H. 2002, in *AMiBA 2001: High-Z Clusters, Missing Baryons, and CMB Polarization, ASP Conference Proceedings, Vol. 257.*, eds.: L.W. Chen et al. (Astronomical Society of Pacific)
 Liao, Y.-W. et al. 2008, ApJ (Lett.), submitted (this issue)
 Lin, K.-Y., Woo, T.-P., Tseng, Y.-H., Lin, L., & Chiueh, T. 2004, ApJ, 608, L1
 Lin, K.-Y. et al. 2008, ApJ, submitted
 Liu, G.-C. et al. 2008, ApJ, in preparation
 Lo, K.Y. et al. 2001, in *AIP Conference Proceedings*, 586, 172
 Markevitch, M. et al. 2000, ApJ, 541, 542
 Mason, B.S., et al. 2003, ApJ, 591, 540
 Mather, J.C. et al. 1990, ApJ, 354, L37
 Molnar, S. et al. 2008, ApJ, in preparation

- Mroczkowski, T. et al. 2008, ApJ, submitted (arXiv:0809.5077)
- Nishioka, H. et al. 2008, ApJ, in press (arXiv:0811.1675)
- Nolta, M. R. et al. 2008, ApJS submitted (arXiv:astro-ph/08030593)
- Okabe, N. & Umetsu, K. 2008, PASJ, 60, 345
- Padin, S. et al. 2002, PASP, 114, 83
- Page, L. et al. 2007, ApJS, 170, 335
- Park, C.-G., Ng, K.-W., Park, C., Liu, G.-C., & Umetsu, K. 2003, ApJ, 589, 67
- Pearson, T.J., et al. 2003, ApJ, 591, 556
- Penzias, A. A. & Wilson, R. W. 1965, ApJ, 142, 419
- Pryke, C. et al. 2008, ApJ submitted (arXiv:astro-ph/08051944)
- Readhead, A. C. S. et al. 2004, Science, 306, 836
- Raphaeli, Y. 1995, ARAA, 33, 541
- Scaife, A. M. M. et al. 2008, MNRAS, 385, 809
- Smoot, G.F. et al. 1992, ApJ, 396, L1
- Spergel, D.N. et al. 2003, ApJS, 148, 175
- Spergel, D.N. et al. 2007, ApJS, 170, 377
- Sunyaev, R.A. & Zel'dovich, Y.B. 1970, Comments Astrophys. Space Phys., 2, 66
- Sunyaev, R.A. & Zel'dovich, Y.B. 1972, Comments Astrophys. Space Phys., 4, 173
- Umetsu, K. & Futamase, T. 2000, ApJ, 539, L5
- Umetsu, K., Chiueh, T., Lin, K.-Y., Wu, J.-M., & Tsheng, Y.-H. 2004, Monder Physics Letters A, 19, 1027
- Umetsu, K. & Broadhurst, T. 2008, ApJ, 684, 177
- Umetsu, K. et al. 2008, ApJ, in press (arXiv:0810.0969)
- Weinreb, S., Lai, R., Erickson, N., Gaier, T., Wielgus, J. 1999, *Microwave Symposium Digest*, 1999 IEEE MTT-S International Volume 1, 101
- White, M., Carlstrom, J.E., Dragovan, M., & Holzappel, W.L. 1999, ApJ, 514, 12
- Wu, J. H. P. 2004, Modern Physics Letters A, 19, 1019
- Wu, J. H. P. et al. 2008a, Modern Physics Letters A, 23, 1675
- Wu, J. H. P. et al. 2008b, ApJ, in press (arXiv:0810.1015)
- Zhang, P., Pen, U.-L., Wang, B. 2002, ApJ, 577, 555

TABLE 1. BASIC CHARACTERISTICS OF THE AMiBA

Components	Specifications
Interferometer elements	7 0.6-meter (13 1.2-meter), $f/2.0$ Cassegrain
Telescope mount	hexapod
Telescope backup structure	6-meter carbon fiber platform
Primary reflector	monolithic carbon fiber
Surface accuracy	30 microns rms
Secondary reflector	carbon fiber, fixed
Array configuration	rings at 0.6m spacings
Available baselines	0.6 - 6.0 meters
Operating frequencies	94 GHz
Maximum angular resolution	2'
Primary beam field of view	23' (11')
Receiver band	86–102 GHz
Number of receivers	7 (13) dual polarization MMIC IP HEMT
Correlator	4-lag analog 2×21 (78) baselines
Point source sensitivity	63 (8) mJy in 1 hour on-source integration

NOTE. — The values in parenthesis will apply after the system upgrade to 13-elements with 1.2-meter antennas. The point source sensitivity here is for two-patch differencing observations.



FIG. 1.— View of the AMiBA telescope on Mauna Loa, in October 2006, during dedication.

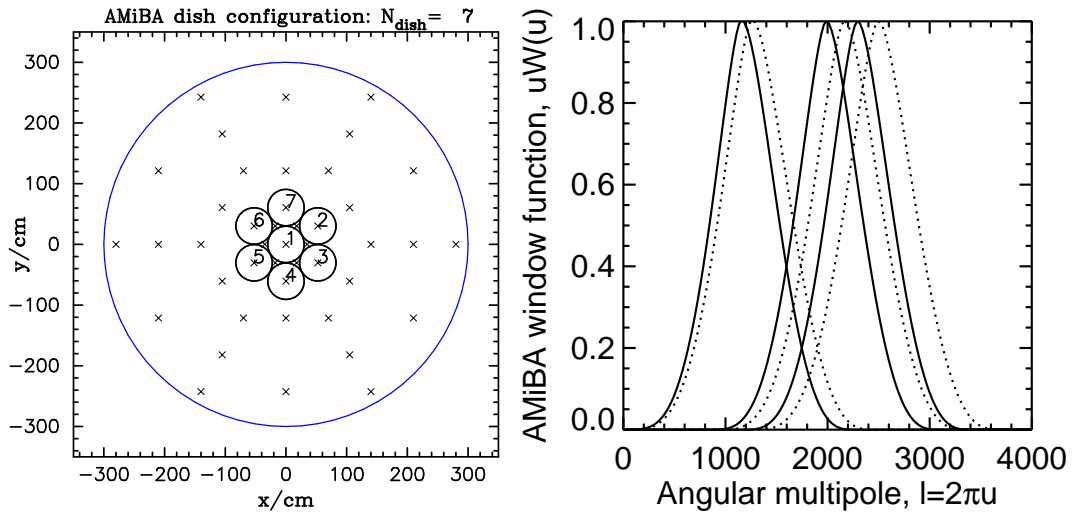


FIG. 2.— *Left*: Initial compact configuration of seven 0.6m antennas (*small solid circles*) on a 6m single platform (*outer solid circle*). *Right*: Sensitivity of the 7-element AMiBA as a function of spherical harmonic multipole $l = 2\pi d/\lambda$ at two frequency channels 90 (*solid*) and 98 (*dashed*) GHz, shown by window functions for three baselines with different lengths (see eq. [14] of White et al. 1999).



FIG. 3.— A close-up of the AMiBA telescope. The left panel shows the initial configuration of seven 0.6 m antennas co-mounted on a 6 m platform. Shown in the right panel are the receiver packages mounted on the platform together with various electronics such as the correlator and LO/IF systems. The reflectors and receivers can be deployed at various locations on the platform in order to achieve different projected baselines.

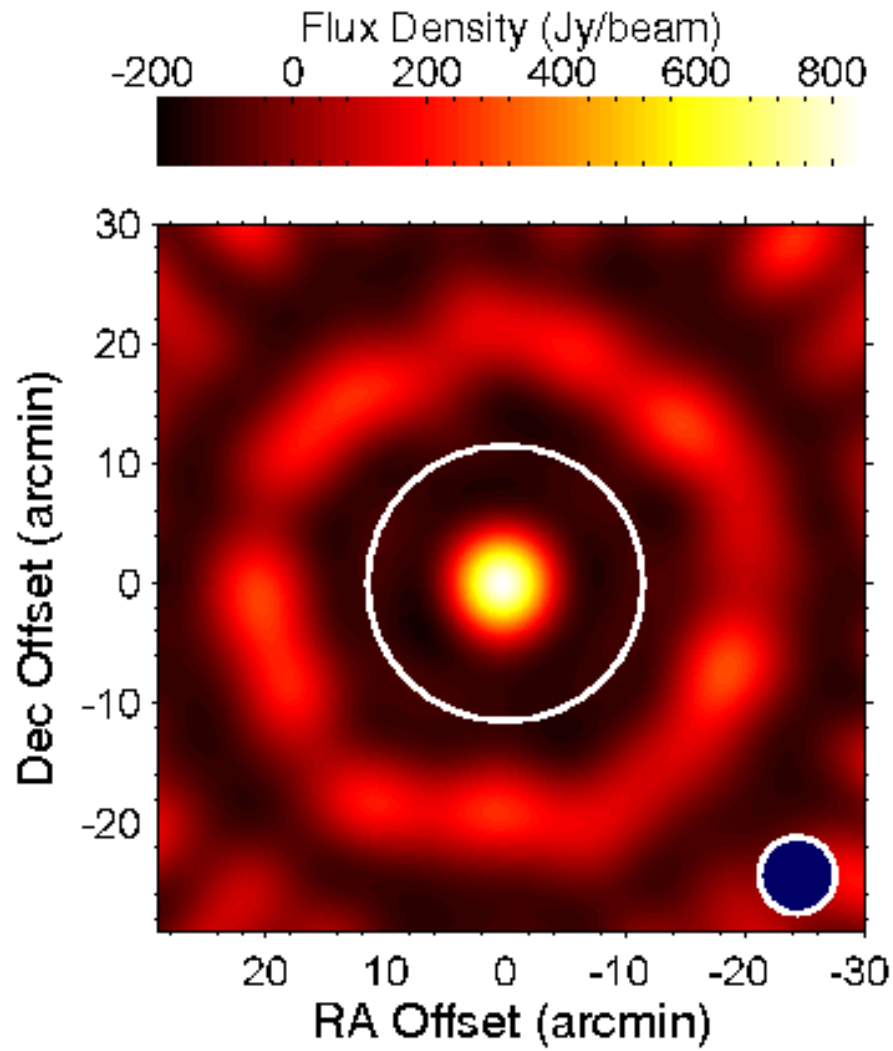


FIG. 4.— The first light image of Jupiter obtained by AMiBA in September 2006. This was a verification of the receiver and correlator systems as well as the pipeline software developed to calibrate and image the interferometer data. This is an un-cleaned, “dirty” image. The white circle indicates the field of view, while the blue region at the bottom-right corner shows the FWHM of the synthesized beam, which is about $6'$.

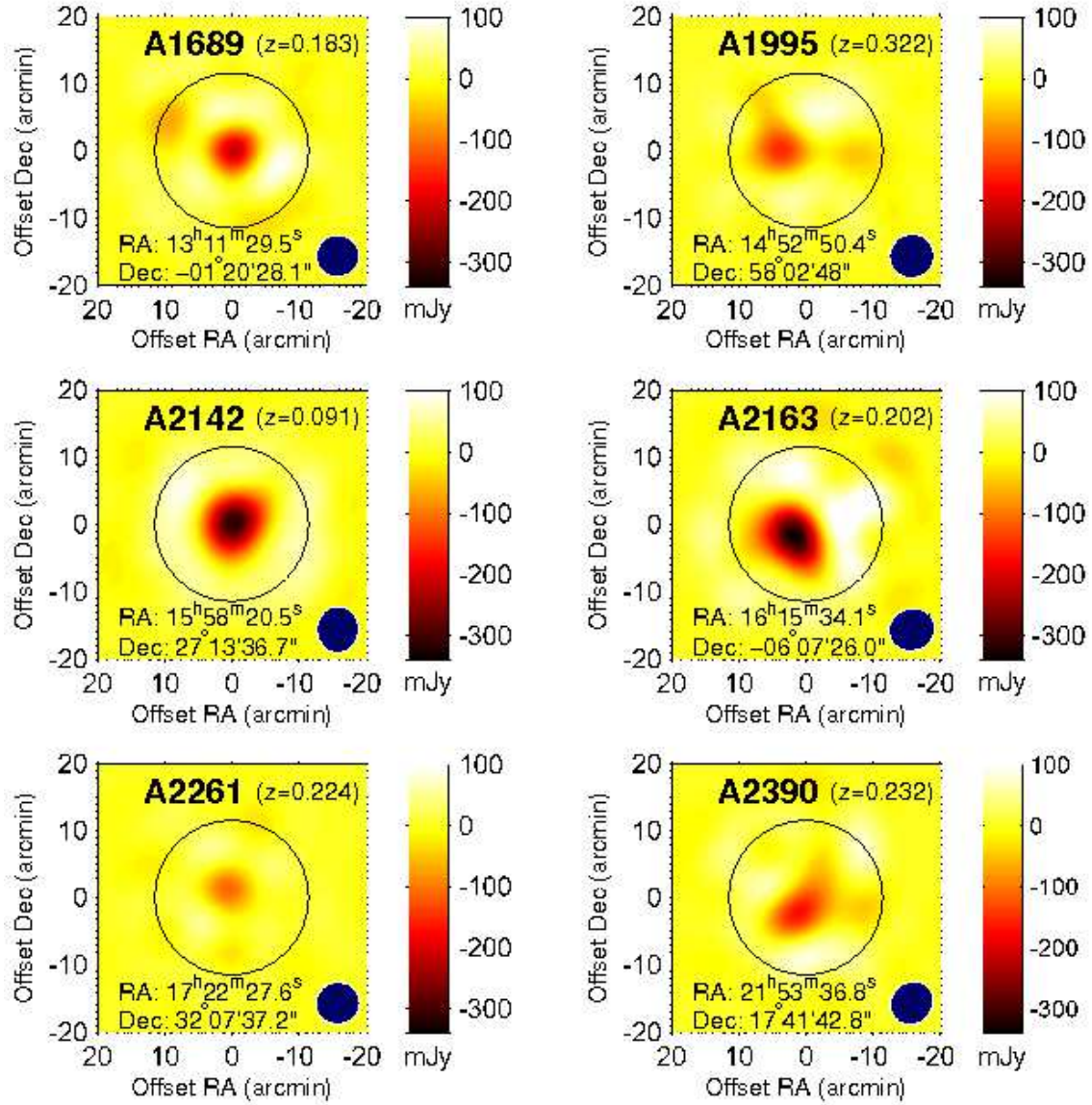


FIG. 5.— The first AMiBA images of the SZE decrement towards six massive clusters of galaxies, A1689, A1995, A2142, A2261, and A2390.

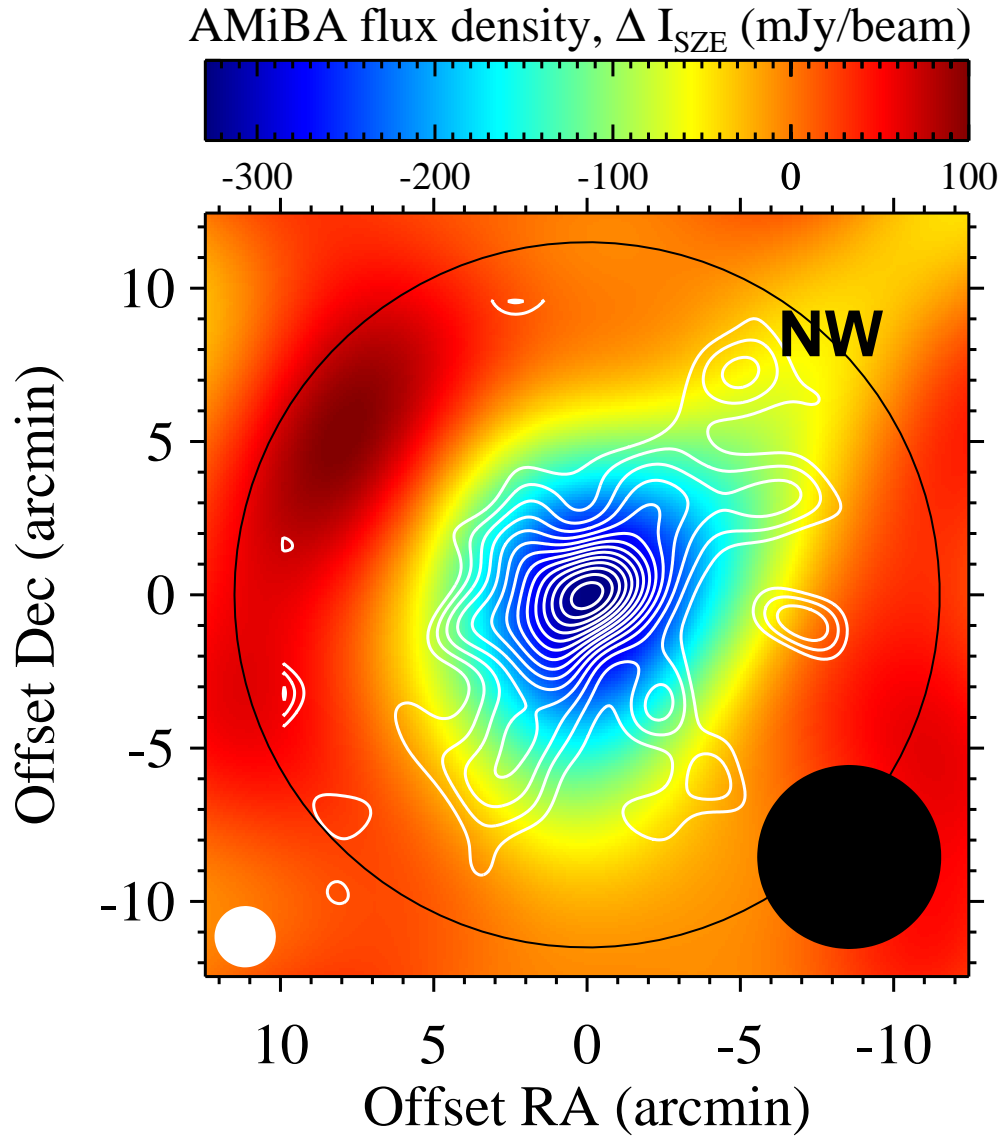


FIG. 6.— The cleaned AMiBA map of the cluster A2142 ($z = 0.091$), revealing a strong SZE decrement of about $-330 \text{ mJy beam}^{-1}$ in the cluster center (Wu et al. 2008b). The field size shown is $25'$, corresponding to $\simeq 1.8 \text{ Mpc h}^{-1}$ at the cluster redshift. The black circle indicates the size of the AMiBA field-of-view ($23'$ FWHM), and the black filled circle at the bottom-right corner shows the size of the AMiBA synthesized beam ($6'$ FWHM). The residual rms noise level in the cleaned map is $\simeq 23 \text{ mJy}$ (Wu et al. 2008b). Overlaid are the contours (*white*) of the projected mass distribution reconstructed from Subaru weak lensing data (see Umetsu et al. 2008; Okabe & Umetsu 2008). The contours are spaced from the 2σ noise level at intervals of 1σ . Shown at the bottom-left corner is the $2'$ FWHM of the Gaussian smoothing kernel (*white filled circle*) used for mass reconstruction. The weak lensing map shows a mass subclump in the northwest region located about $10'$ northwest from the cluster center. A slight excess of the SZE signal, extending in the northwest direction, is seen in the northwest region at $2-2.5\sigma$ levels.